Available online at www.sciencedirect.com
ScienceDirect
Ceramics International 38 (2012) 941–949
CERAMICS INTERNATIONAL
www.elsevier.com/locate/ceramint

A facile synthetic strategy for Mg–Al layered double hydroxide material as nanocarrier for methotrexate

Manjusha Chakraborty [a], Sudip Dasgupta [a], Somoshree Sengupta [a], Jui Chakraborty [a], Swapankumar Ghosh [b,*], Jiten Ghosh [a], Manoj Kumar Mitra [c], Akhilesh Mishra [d], Tapan Kumar Mandal [d], Debabrata Basu [a]

[a] *Central Glass & Ceramic Research Institute, CSIR, 196 Raja S.C. Mullick Road, Kolkata 700032, India*
[b] *National Institute for Interdisciplinary Science & Technology (NIIST), CSIR, Trivandrum 695019, India*
[c] *Department of Metallurgical and Materials Engineering, Jadavpur University, Kolkata 700032, India*
[d] *Department of Veterinary, Pharmacology and Toxicology, West Bengal University of Animal and Fisheries Sciences, 68 K.B. Sarani, Belgachia Road, Kolkata 700037, India*

Received 16 May 2011; received in revised form 4 August 2011; accepted 8 August 2011
Available online 22 August 2011

Abstract

Mg–Al layered double hydroxide nanopowders were synthesised by a facile coprecipitation technique at different pH conditions. LDH nanoparticles of higher aspect ratio with an average particle size of 26 nm were obtained at pH 9 whereas a pH of 11.3 resulted in LDH nanoparticles of average size 50 nm with lower aspect ratio and narrower size distribution. LDH–MTX organo–inorganic nanohybrid was produced with an average particle size of 53 nm after intercalation of MTX into the interlayer space of LDH, as evident from the shift of (0 0 3) peak in X-ray diffraction. This was corroborated by the transmission electron micrograph, which showed an increase in average interlayer spacing from 8.00 Å in pristine LDH to 21.4 Å in LDH–MTX nanohybrid. Thermogravimetric analyses showed ~33.2 wt% MTX loading in the LDH structure. The MTX release profile from Mg–Al LDH–MTX nanohybrid in phosphate buffer saline at pH 7.4 follows Ritger–Peppas kinetics model which demonstrates that the release kinetics is diffusion controlled. An attempt has been made to explain the above observations based on the effect of electrical double layer repulsions on the growth of LDH nuclei, primarily considering significance of the particle morphology in drug delivery application.

Keywords: B. Platelets; E. Biomedical applications; Layered double hydroxides (LDH); A. Chemical precipitation

1. Introduction

Numerous efforts have been made in recent times to develop novel drug carrier for transport, storage and release, which exhibit numerous advantages over the conventional forms of dosage, such as enhanced bioavailability, greater efficacy and safety, controlled and prolonged release time, and predictable therapeutic response [1]. So far, a large number of materials have been employed as various drug delivery systems, such as biodegradable polymers, hydroxyapatite, xerogels, hydrogels [1], guar gum nanoparticles [2], fluoride hollow structures [3], superparamagnetic nanoparticles [4,5], functionalized mesoporous materials [6–8] and layered double hydroxides (LDHs) [9]. LDHs are considered to be the new generation materials, comprising two dimensional layered structure similar to that of mineral brucite, $Mg(OH)_2$ [10]. LDHs have many other properties which make them attractive for real applications; these include nanomedicine [10,11], catalyst supports [11,12], agriculture, pharmaceuticals, and detergent manufacturing [13]. Mg–Al layered double hydroxide (LDH) is a good reservoir for different kind of drugs in their anionic form [14–17] and is of particular interest in the field of cellular delivery of drug and biomolecules. LDH nanoparticles are reported to be easily endocytosed inside the cellular compartments based on their size and morphology [18,19]. Intensive investigations in

* Corresponding author. Tel.: +91 33 24733469x3233; fax: +91 33 24730957.
E-mail addresses: jui@cgcri.res.in (J. Chakraborty), swapankumar.ghosh2@mail.dcu.ie (S. Ghosh).

0272-8842/$36.00
doi:10.1016/j.ceramint.2011.08.014

the area of targeted drug delivery to combat with cancer disease has prompted the use of LDHs [20], that have a cationic framework formed by the isomorphous substitution of M^{2+} (where M is Mg, Ca, Zn Fe, Cu, Mn, etc.) ions, with M^{3+} (where M is Al, Fe, Cr, Co, etc.) ions in the structure of $M^{2+}(OH)_2$ [11]. The incorporated drugs inside the LDH nanocarriers would possess higher resistance to enzymatic degradation, do not easily desorb away in the blood circulation and thus can be targeted to specific cells and tissues.

The shape or morphology of nanocarrier plays an important role in drug transport to specific cells or tissues and subsequent endocytosis inside the cellular compartments. Interaction of spherical particles with cells of animals has been studied extensively [21,22], but the effects of shape have received little attention. Depending on the requirements, the shape of nanocarrier can be tailored and transport to specific targets can be made faster or slower [23,24]. The size of nanoparticles used in a drug delivery system should be optimum to prevent their rapid release into blood capillaries but small enough to escape capture by fixed macrophages that are lodged in the reticuloendothelial system, such as the liver and spleen and reach tumor tissues [25,26]. There is substantial progress in preparation, application and perspectives of LDHs with different morphologies. Kuang et al. have summarized the progress in fabrication of range of LDH morphologies from spherical, one-dimensional (1-D) belt/fiber to 2-D films [27]. Further, they have mentioned that LDH nanopowders synthesized by conventional coprecipitation technique showed preferential growth of the *a–b* plane to form hexagonal platelet morphology. Lu et al. have correlated the relationship between particle morphology and hydrothermal treatment conditions, e.g. time, temperature and concentration [28]. To the best of our knowledge, no attempt has been made to elaborate the effect of precipitating pH conditions on the formation of LDH nanocrystals of different morphology.

In view of the above, this communication reports a simple but useful method to prepare stable homogeneous LDH suspensions with controllable morphology by pH variation of the precursor solution at 25 °C. The particles have a narrow size distribution in nanoscale. MTX, an anticancer drug is intercalated into the LDH framework by anion exchange technique. The Mg–Al LDH and LDH–MTX composites were characterized using powder X-ray diffraction (XRD), transmission electron microscopy (TEM), Fourier transform infrared spectroscopy (FTIR) and particle size analysis. The extent of intercalation is studied by thermogravimetric analyses (TG). The drug release kinetics was diffusion controlled as evidenced from the best fit into the Ritger–Peppas model.

2. Experimental

2.1. Synthetic methods

All the chemicals used were of analytical grade. Magnesium nitrate hexahydrate $Mg(NO_3)_2{\cdot}6H_2O$ (99%), aluminium nitrate nonahydrate $Al(NO_3)_3{\cdot}9H_2O$ (99%) and sodium hydroxide NaOH (pellets) were purchased from Merck, India. Methotrexate (MTX) was procured from Sun Laboratory (Bangalore, India). Ultrapure decarbonated water (Millipore, specific resistivity 18 MΩ, decarbonated in XL grade nitrogen atmosphere) was used in all the experiments.

Two sets of Mg–Al LDHs were synthesized chemically by co-precipitation route [23] by addition of an aqueous solution of 0.01 M NaOH drop-wise to a 250 ml solution containing 66 mmol $Mg(NO_3)_2{\cdot}6H_2O$ (Sigma–Aldrich) and 33 mmol $Al(NO_3)_3{\cdot}9H_2O$ (Sigma–Aldrich) at 25 °C to obtain the pHs of 9 and 11.3. The reaction was carried out in nitrogen atmosphere while strong magnetic stirring. The stirring was continued for further 1 h to get white gelatinous LDH precipitate. The precipitate was collected by centrifugation and washed repeatedly by redispersing it in water followed by centrifugation to remove excess nitrate ions. The washed LDH precipitates were freeze dried (EYELA, FDU2200, Japan) at −82 °C and 20 Pa pressure to get dry Mg–Al LDH nanopowder. The product obtained at pH 9 will be referred to as LDH9 and pH 11.3 as LDH11. A part of the sample synthesized at pH 11.3 (LDH11) was used for intercalation with methotrexate as described below. Powder LDH11 was chosen for the intercalation of drug on account of its thermodynamic stability with minimum surface charge at the given pH condition close to the isoelectric point (pI) of LDH. About 50 ml 0.043 M methotrexate (MTX) solution was prepared by dissolving MTX in ammoniacal decarbonated water (pH 7.5). MTX solution, so prepared was added to 100 ml aqueous suspension containing 1 g (commensurate with the equivalent amount of nitrate ions) LDH11 under nitrogen atmosphere followed by drop-wise addition of 0.01 M NaOH until the pH was raised to 10. The whole process was carried out with continuous stirring and the reaction mixture was agitated for further 72 h. The resultant suspension of LDH–MTX was centrifuged, washed thrice using decarbonated water and finally freeze dried at −82 °C and 20 Pa pressure. This sample is named as LDH–MTX.

In vitro drug release was studied, as described elsewhere [29], by dispersing 10 mg of Mg–Al LDH–MTX in 30 mL phosphate buffer saline (PBS) of pH 7.4 at 37 °C. An aliquot of 1 mL was taken for analysis and was replenished to keep the final volume constant. It was filtered through a 0.2 μm membrane filter paper. 20 μL aliquots of the filtered solution were analyzed by HPLC using Tris buffer (0.1 M KH_2PO_4 and 0.01 M Tris–HCl), acetonitrile and methanol in 80:10:10 ratio (v/v) as eluent.

2.2. Characterisation techniques

Powder X-ray diffraction patterns of Mg–Al LDH and Mg–Al LDH–MTX were obtained with X'Pert Pro MPD Diffractometer (Panalytical, Almelo, The Netherlands) using Cu Kα (λ = 1.5418 Å) radiation at 40 mA, 40 kV. Powder samples (LDH9 and LDH11) were scanned in the 2θ range 8–70° in 0.03° steps, with a count time of 2 s at each point. LDH–MTX was scanned in the 2–30° (2θ) range. Particle size, morphology and crystallographic analyses of pristine LDHs and MTX intercalated nanohybrid were studied using transmission electron microscopy (FEI Tecnai F30 G^2 S-Twin, The Netherlands)

operated at 300 kV. Grid for TEM study was prepared by dropping a micro droplet of suspension of LDH powder in isopropyl alcohol on to a 400 mesh carbon-coated copper grid and drying the excess solvent naturally. Microanalysis of the samples (elemental composition) were performed using energy dispersive spectroscopy (EDS) with a low system back ground (<1% spurious peaks), high P/B ratio (Fiori number >4000) having spectrum imaging with Si–Li detector attached to the TEM equipment. Thermogravimetric analyses (TG/DTA) of sample powders were carried out at 10 °C/min heating rate in air from ambient to 1000 °C using NETZSCH STA 409 CD simultaneous thermal analyzer. Fourier transform infrared (FTIR) spectra of the as-prepared powders were recorded at room temperature using the KBr (Sigma–Aldrich, ≥99%) pellet method (sample:KBr = 1:100) on a Perkin-Elmer Spectrum 100 spectrophotometer in the 400–4000 cm^{-1} range with average of 50 scans. Particle size distribution and zeta potential measurement were performed at 25 °C using photon scattering, also known as photon correlation spectroscopy (PCS) method in a Zetasizer, Zetatrac (Microtrac, Montgomeryville, PA, USA) with dilute suspensions of LDHs and LDH–MTX. The zetasizer was equipped with 180° back scattering technology for measurement of both low and high scattering (0.01–40%) dispersion systems having accessory for powder and FLEX operating software with two solid state 5 mW diode lasers, operating at a wavelength of 780 nm. HPLC (Shimadzu LC-20AT, Japan) was used to determine the release kinetics of methotrexate drug from LDH–MTX nanocomposite in PBS at pH 7.4.

3. Results and discussion

The powder X-ray diffraction patterns of LDH9, LDH11 and LDH–MTX are shown in Fig. 1. Almost all characteristic diffraction peaks of a hexagonal Mg–Al LDH matching with the JCPDS pattern (JCPDS File No. 35-0964) were observed, with rhombocentered lattice. The peaks corresponding to the higher order reflections are indexed. For the present study, we considered (0 0 6) reflection for single profile analysis to calculate crystallite size (D_{XRD}) and lattice strain (ε) of the LDH samples because (0 0 3) and (0 0 6) reflections are the diffraction lines

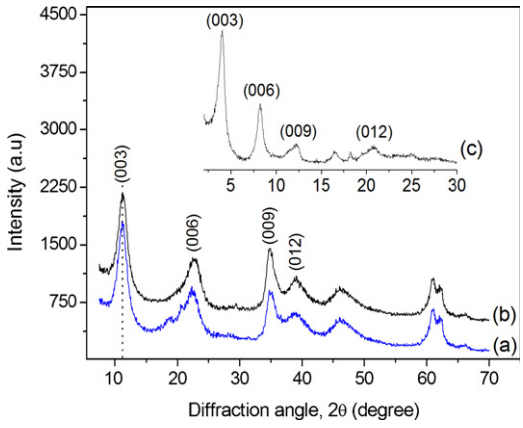

Fig. 1. Powder X-ray diffraction patterns of (a) LDH9, (b) LDH11, and inset (c) LDH–MTX.

corresponding to different orders of reflections from the same plane appeared in the observed XRD patterns (Fig. 1).

The lattice-strain was calculated with respect to the second order reflection (0 0 6) only, because of asymmetric shape of the first order reflection (0 0 3). The crystallite size and lattice strain of the LDH samples were calculated by the two well known Scherrer formulae [30,31]

$$\text{Crystallite size} = \frac{k\lambda}{\beta \cos\theta}, \quad (1)$$

$$\text{Lattice strain, } \varepsilon = \frac{\beta}{4 \tan\theta}, \quad (2)$$

where β (size) = $\beta_{obs} - \beta_{std}$ and β (strain) = $\sqrt{\beta_{obs}^2 - \beta_{std}^2}$, λ is the wavelength of incident X-ray, θ is the diffraction angle for the (0 0 6) plane, and k is a constant (shape factor) and has a value of 0.89. Here β describes the structural broadening, which is the difference in integral profile width between a standard (β_{std}) and the experimental sample (β_{obs}). For XRD line profile analysis, NIST 660a was taken as the standard sample, which did not have any size and/or strain broadening, to encompass the effect of instrumental broadening of the diffractometer. It is evident from the lattice strain along (0 0 6) crystallographic direction, that LDH9 has approximately 1.29% more strain than that in LDH11 (Table 1). This may be attributed to the excess positive charge density in the *a–b* plane as mentioned above which leads to repulsion between the planes in the *c*-direction and hence inhibition of growth along the same, resulting in an elongated, exfoliated morphology of the particles.

Due to intercalation of MTX into interlayer space of LDH, the *d*-spacing for basal planes ($d_{0\,0\,3}$) increased from 8.01 Å in pristine LDH to 21.6 Å in LDH–MTX nanohybrid as the peak corresponding to (0 0 3) plane shifted from 11.05° 2θ to 4.08° 2θ [32] as shown in Fig. 1. The increase in the LDH gallery height is due to the replacement of change balancing nitrate ions with large MTX anions in the interlayer space. The brucite sheet thickness of Mg–Al LDH is reported as 4.8 Å [29,33]. The ($d_{0\,0\,3}$) enhancement on intercalation can be estimated as 16.8 Å which is always smaller than the longitudinal MTX molecular length (21.2 Å) because of its tilted spatial configuration in Mg–Al LDH–MTX [29]. The intercalation of MTX into the interlayer space of LDH was also confirmed from high-resolution transmission electron microscopy (HR-TEM) images given in Fig. 2. The average thickness between two corresponding layers in pristine LDH11 is ∼8.00 Å (Fig. 2A) which increased to 21.4 Å in LDH–MTX nanohybrid (Fig. 2B) after intercalation of MTX into interlayer space of LDH.

Table 1
Crystallite size and lattice strain data of LDH11 from single profile analysis using Eq. (2).

Sample	Size-strain along (0 0 6) crystallographic direction	
	Crystallite size (nm)	Lattice strain (%)
LDH9	4.1	7.651
LDH11	4.5	6.361

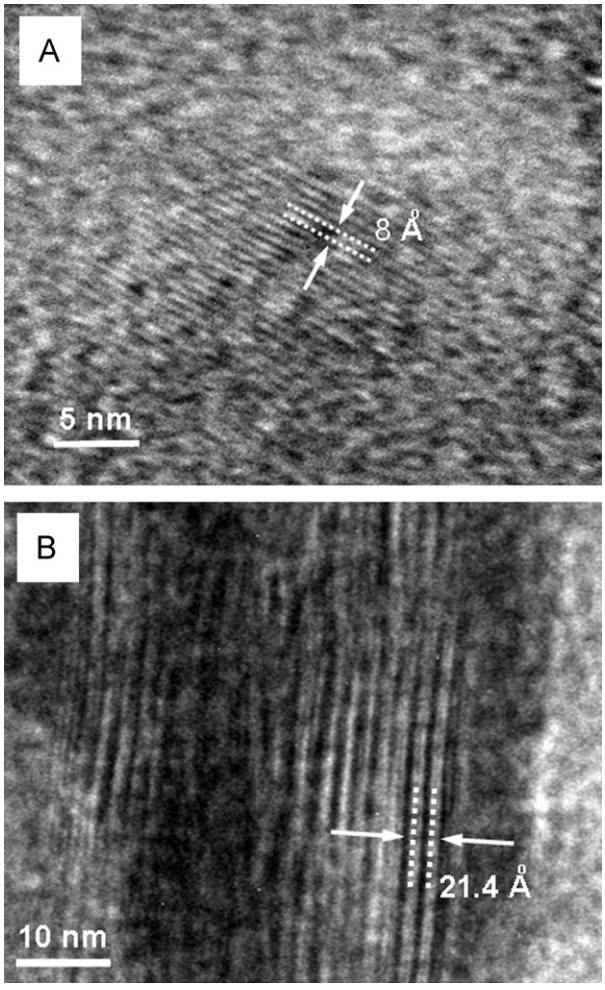

Fig. 2. HR-TEM image of (A) LDH11 indicating distinct crystal facets and (B) LDH–MTX.

Fig. 3 shows the bright field TEM micrographs of LDH9 and LDH11. Highly exfoliated clay particle type of morphology (arrow marked in Fig. 3A) having high aspect ratio (length:width > 30:1), was observed in LDH9, whereas hexagonal platelet shaped LDH nanoparticles were found in LDH11 (Fig. 3B). The average size of LDH9 particles synthesized at pH 9 is calculated as 27.5 nm from multiple TEM images whereas the LDH11 contains much larger particles of average size ~49.5 nm (Fig. 3). The SAED patterns [inset, Fig. 3A and B)] show Debye-Scherrer rings corresponding to the diffraction from the characteristic atomic planes (1 0 1), (1 1 0), (0 0 9) and (0 1 1 1) planes of LDH nanoparticles.

The EDS data (Table 2) of LDH9 and LDH11 exhibit the presence of both Mg and Al ions in the composition. Small crystallite sizes (D_{XRD}) of 4.1 nm for LDH9 and 4.5 nm for LDH11 (Table 1) indicate that LDH particles are polycrystalline.

It is evident from the EDS of LDH9 (Table 2) that the Mg:Al molar ratio is close to unity (1.08). This is attributed to the incomplete precipitation of Mg^{2+} ion at pH 9.00 specifically leading to an increase in positive charge density in the *a–b* plane (Fig. 3) due to the excess Al^{3+} ions. This in turn inhibits stacking of the LDH layers in the *c*-direction that corroborates the schematic model of the same as discussed later (Scheme 1).

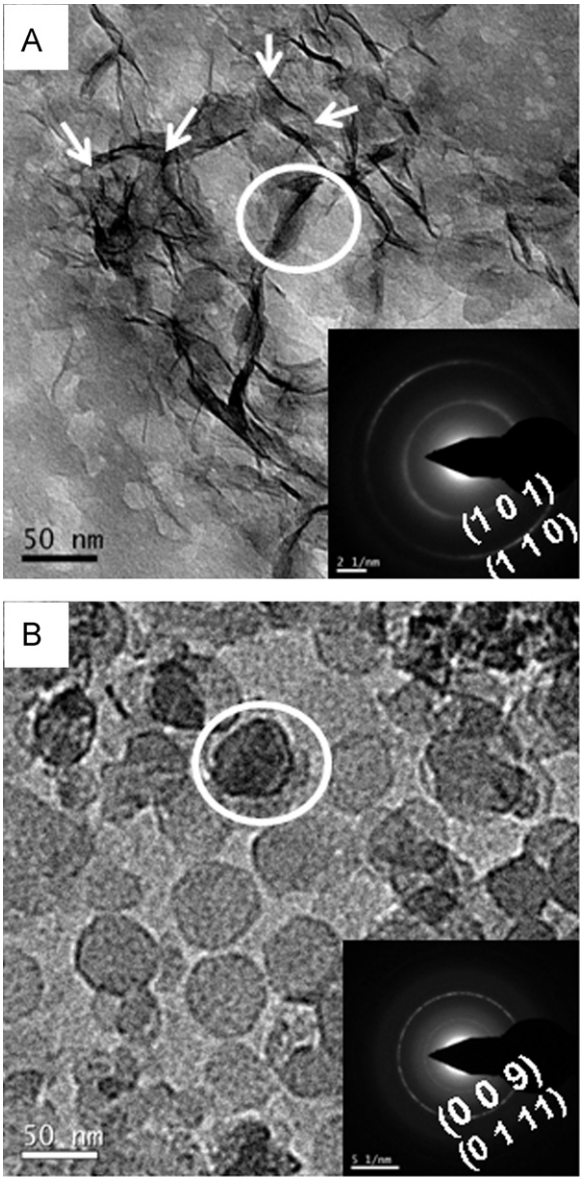

Fig. 3. TEM images of Mg–Al LDH nanopowders synthesized using coprecipitation method at different pH: (A) 9 and (B) 11.3. SAED patterns exhibiting the presence of characteristic Debye–Scherrer rings are shown in both the images as insets.

For LDHs, the atoms within the sheets (*a–b* plane) are covalently bonded and molecular slabs are stacked together by electrostatic forces between brucite-like sheets and inter anions along the *c*-axis [34]. After addition of NaOH in the precursor solution the Mg–Al LDH nuclei were formed and growth of these nuclei took place through edge sharing (*a–b* plane) and

Table 2
Micro elemental analysis of LDH9 and LDH11 from TEM.

Sample	Element	Weight (%)	Atomic (%)
LDH9	Mg	45.24	47.19
	Al	46.42	43.61
LDH11	Mg	55.25	60.70
	Al	32.72	30.24

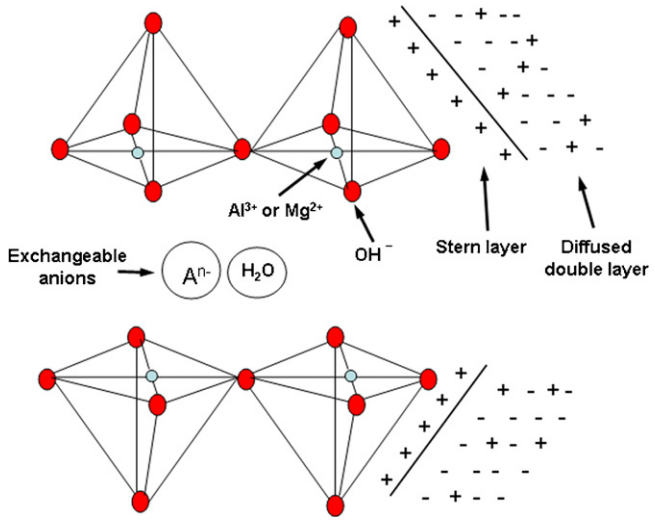

Scheme 1. Schematic representation of structure and electronic charge distribution in LDH in aqueous suspension with pH lower than the isoelectric point.

stacking (*c*-axis) of the lattices. Intra layer bonding in LDH is typically strong in nature while the interlayer interactions are governed by weaker forces such as electrostatic interactions, H bonding etc. Stacking of LDH on top of each other is kinetically favoured, though the growth of LDH nanocrystal in *a*–*b* plane is thermodynamically more favourable [35]. At pH lower than the isoelectric point, (pI of LDH ∼11.3) [36] LDH nanoparticles were covered with positively charged stern layer followed by a diffused electrical double layer (Scheme 1). The brucite layers in Mg–Al LDH are itself positively charged and thus electrostatic attraction (from the negatively charged interlayer anions, e.g., nitrate anion) and repulsion played a major role in the growth of LDH nuclei. At pH 9, due to electrical double layer repulsion among LDH nuclei (the substantially high value of zeta potential, 39.86 mV, indicates significant amount of electrical double layer repulsion between the positively charged layers), stacking of the lattices in the *c*-direction became energetically less favourable, and the LDH nuclei grew preferentially in the *a*–*b* plane to maximize energy gain from the iono-covalent interactions between LDH sheets (Scheme 2A). This phenomenon led to growth of the LDH nanoparticles in a layer like morphology with high aspect ratio. On the contrary, as we go close to isoelectric point of LDH (pI ∼ 11.3), there exists very weak or no electrical double layer repulsion as indicated by the zeta potential data (−2.99 mV, data not provided here), that corresponds to a very low value almost close to zero. Hence, the LDH nuclei grew uniformly from all directions to give low aspect ratio, platelet like morphology of the LDH nanoparticles that minimises the surface energy (Scheme 2B).

Thermogravimetric analyses (TG/DTA) of pristine LDH11, LDH–MTX and pure MTX powder are shown in Fig. 4 which shows total weight loss of 36.5, 54.9, and 92% respectively on heating to 1000 °C. Weight loss in LDH11 as well as MTX intercalated LDH–MTX occurred mainly in two temperature regions around 200 °C and 430 °C because of dehydroxylation of water molecules and decomposition of organic and inorganic anions intercalated and bound to cationic sheets respectively. Nearly 11 wt% loss in pristine LDH and 15% in LDH–MTX are attributed to dehydroxylation of physisorbed and structural water molecules respectively on heating up to 225 °C. The weight loss in pristine Mg–Al LDH sample increased to 36.5% on heating up to 600 °C because of decomposition of interlayer nitrate and carbonate anions. LDH–MTX showed a weight loss of ∼53% on heating up to 600 °C because of decarboxylation of methotrexate and decomposition of remaining nitrate and other charge balancing anions. On heating to 800 °C, the rest ∼2% weight loss is due to dehydroxylation during spinellization from layered double hydroxide and oxide based lattice structure [37]. Thermogravimetric analyses showed ∼33.2 wt% MTX loading in the LDH structure. Differential thermal analysis profiles of pristine LDH11 and LDH–MTX nanohybrid are presented in Fig. 5. Removal of loosely bound physically adsorbed water was marked by the endotherm at ∼100 °C whereas endothermic dehydroxylation due to removal of hydrogen bonded structural water occurred at 240 °C. Endothermic decomposition of bound nitrate and carbonate to the cationic framework of LDH11 occurred at around 435 °C, whereas in LDH–MTX nanohybrid the endothermic peak because of decarboxylation of intercalated and bound methotrexate anions in the interlayer as well as on the edges and faces of cationic brucite sheets appeared at ∼420 °C. Spinellization in pristine Mg–Al LDH started with the expulsion of Al^{3+} ions from MgO nanocrystals, as marked by the broad endothermic peak at 700 °C. Spinellization in LDH–MTX nanohybrid occurred at a higher temperature of 850 °C as compared to that in pristine LDH because of the presence of trace amount of organic molecules that acted as a barrier for diffusion of Al^{3+} ions and nucleation of $MgAl_2O_4$ spinels [38,39]. Strain energy of MgO nanocrystals decreased on decarboxylation and decomposition of methotrexate which was reflected in a small endothermic hump at 550 °C [40].

FTIR spectra of LDH11, MTX material and LDH–MTX nanohybrids are shown in Fig. 6. Lattice vibrations due to the presence of metal–oxygen and metal–hydroxyl bonds were detected at 600 and 428 cm^{-1} respectively. The band at 1384 cm^{-1} corresponding to stretching vibration of NO_3^- ions in Mg–Al LDH structure was found to be less intense in nanohybrid which suggests a decrease in nitrate ion concentration in LDH–MTX hybrid as compared to that in pristine LDH. The absence of any detectable band at 1357 cm^{-1} reveals the fact that no CO_3^{-2} anion was present in Mg–Al LDH. MTX intercalated Mg–Al LDH nanohybrid showed symmetric and asymmetric stretching vibration of COO^- (νCOO^-) at 1373 and 1565 cm^{-1} respectively. The stretching vibrations at 1405 and 1606 cm^{-1} appeared due to C=C stretching of MTX in LDH–MTX nanohybrid. The band at 1606 cm^{-1} in the nanohybrid signifies the presence of C=O stretching. These suggest the presence of methotrexate in LDH–MTX nanohybrid [41,42]. The absorption band in the broad range of 3200–3400 cm^{-1} signifies the stretching vibration of labile hydroxyl group or physically adsorbed water molecule in Mg–Al LDH which was found to be very sharp and intense in case of LDH–MTX nanohybrid [42]. Intercalation of MTX into the interlayer

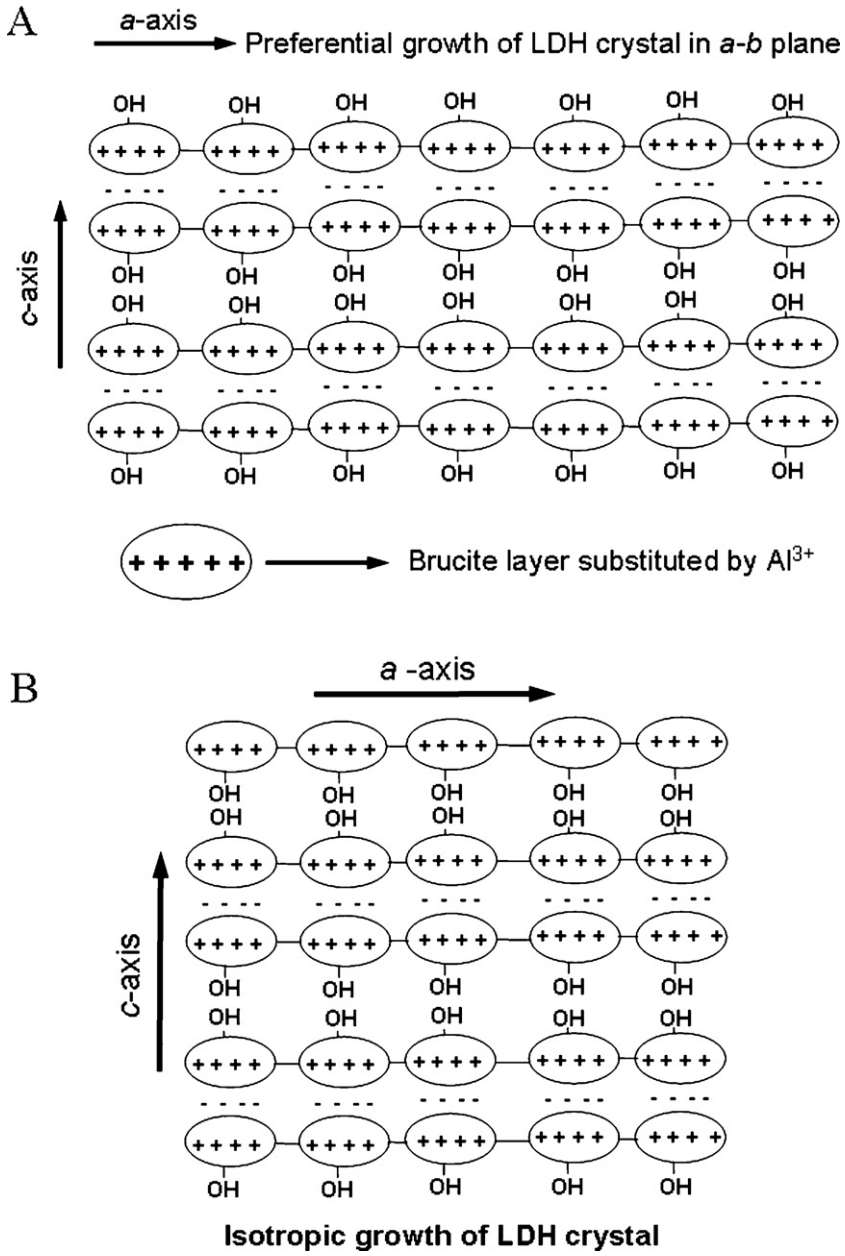

Scheme 2. Schematic representation of growth of Mg-Al LDH nanocrystal at (A) pH 9, and (B) pH 11.3.

space of Mg–Al LDH resulted in more directionality in the interatomic interactions where crystalline and adsorbed water molecules could closely be attached to the structure through more homogeneous hydrogen bonding interactions [43].

The hydrodynamic sizes of pristine and methotrexate intercalated Mg–Al LDH in aqueous suspension, measured by light scattering is given in Fig. 7. The size profile of LDH9 shows a closely overlapping bimodal distribution of sizes in the range 15–100 nm with average size ~26 nm as compared to an average particle size of 50 nm obtained for LDH11. Size data from PCS for LDH9 and LDH11 validates the sizes estimated for them from TEM measurements (Fig. 3). Due to the presence of electric double layer repulsion between LDH particles, *c*-axial stacking of the crystallites is hindered at pH 9 in the reaction mixture and resulted in a lower particle size with exfoliated type morphology in LDH9. On the contrary, nanoparticles (LDH11), synthesized at pH close to its isoelectric point (pH 11.3), growth of LDH crystallites occurred uniformly from all directions and that led to the formation of more or less isotropic growth of LDH nanoparticles with larger average size (50 nm). On intercalation of MTX, the resultant LDH–MTX nanohybrid showed a little larger size of ~53 nm because of increase in the gallery height due to the incorporation of MTX.

Fig. 8 shows the cumulative release of MTX from LDH–MTX nanohybrid in phosphate buffer saline at pH 7.4. The initial burst release of 26 wt% of MTX in 2 h incubation in PBS solution was due to desorption of loosely bound MTX from the surface of LDH–MTX nanohybrid. This was followed by a constant rate of release of 14 wt% MTX in a period of 2–4 h due to detachment of strained MTX molecule bound to LDH lattice.

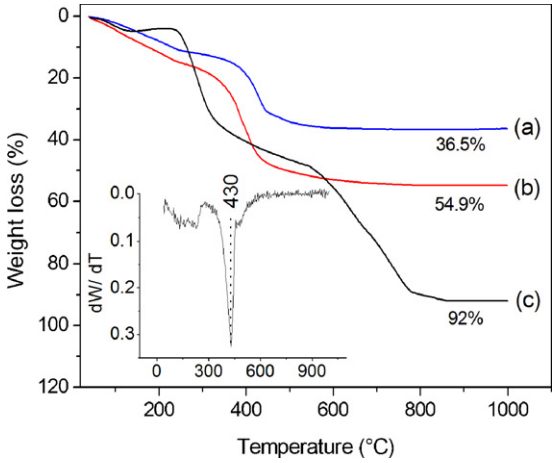

Fig. 4. Thermogravimetric analyses of (a) LDH11, (b) LDH–MTX, and (c) MTX. Derivative of TG plot of LDH11 is given in inset.

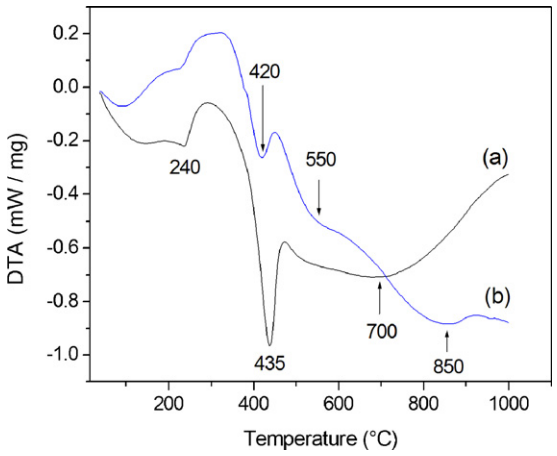

Fig. 5. Differential thermal analyses of (a) LDH11 and (b) LDH–MTX.

Release of MTX up to 22 wt% within a period of 4–8 h of incubation in PBS was due to deintercalation of anionic drug from interlayer space because of the electrostatic interaction between anionic species in PBS including carbonate and bicarbonate coming from air and cationic octahedral framework.

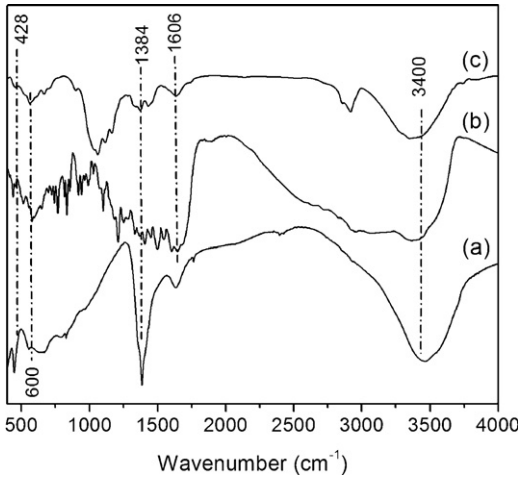

Fig. 6. FTIR spectra of (a) LDH11, (b) MTX, and (c) LDH–MTX.

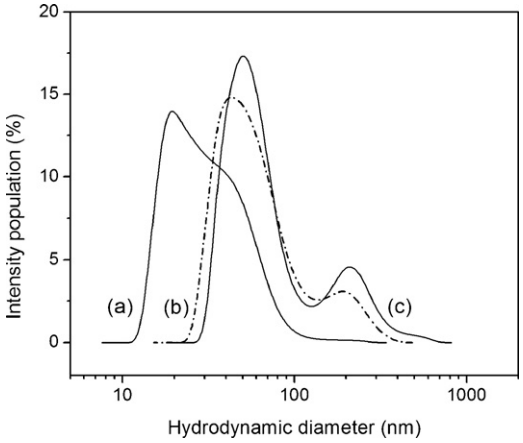

Fig. 7. Particle size analysis of LDH nanoparticles prepared: (a) LDH9, (b) LDH11, and (b) LDH–MTX hybrid.

The release of next 13 wt% MTX occurred linearly up to a period of 12 h of incubation of LDH–MTX nanohybrid in PBS due to a combination of deintercalation of MTX and crystal dissolution of LDH–MTX nanohybrid. A very slow release of rest 25 wt% of MTX up to a period of 120 h was primarily because of detachment of tightly bound MTX molecule in course of gradual dissolution of LDH–MTX nanohybrid at pH 7.4.

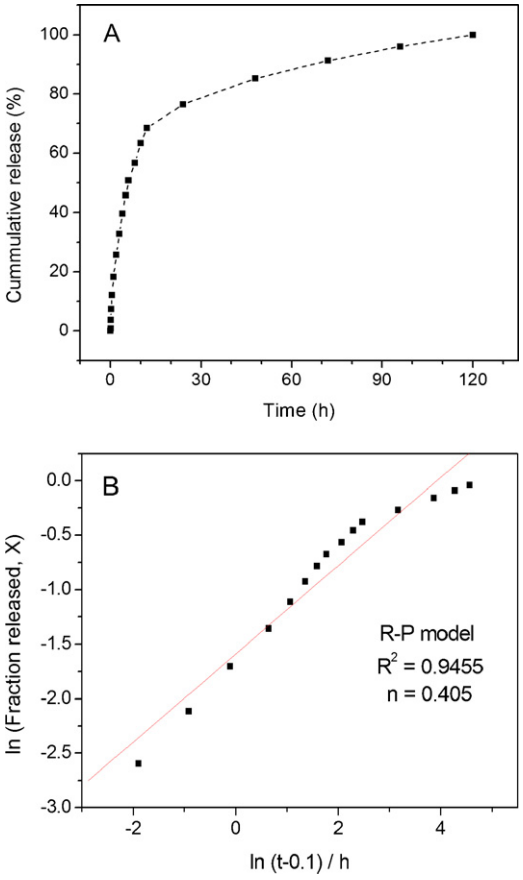

Fig. 8. (A) Cumulative release rate of MTX from LDH–MTX nanohybrid at 37 °C and (B) fit of cumulative released fraction of MTX from LDH–MTX nanohybrid with respect to incubation time (t) following Rigter–Peppas model.

Cumulative release kinetic of MTX from LDH–MTX nanohybrid was fitted into Rigter–Peppas model [29], following equation $X = k(t - \alpha)^n$, where X, t, k, α and n are the drug release (%), release time, kinetics constant, modified parameter, and an exponent respectively. The exponent n, is normally used to describe different release mechanisms. The value of exponent n was estimated to be 0.405. Value of $n < 0.45$ indicates that the release behaviour of MTX from LDH–MTX nanohybrid is predominantly diffusion controlled [29,44] in phosphate buffer solution of pH 7.4.

4. Conclusions

A pH dependent variation in morphology of Mg–Al LDH nanopowder and its plausible explanation has been discussed in this study. Presence of surface charge at precipitation pH 9 resulted in LDH with lower particle size in 10–100 nm range in LDH9 whereas isotropic growth at pH close to its isoelectric point produced larger particles in 25–290 nm range in LDH11. Estimated lattice strain from XRD in LDH9 is 1.29% more than the same in LDH11. This observation was supported by the EDS analysis which indicates incomplete precipitation of Mg^{2+} ion in presence of Al^{3+} ion that reasonably enhances the positive charge density and hence growth along the *a–b* axis only. Loading of MTX in to the cationic framework of LDH11 to the extent of ∼33.2% obtained from TG data and the release profile showed efficient intercalation. Cumulative MTX release from the LDH galleries in PBS (pH 7.4) medium was ∼76% in 24 h at 37 °C and the entire MTX was released in a period of 120 h. Rigter–Peppas kinetics model provided a good description for the release process demonstrating that the MTX release was mainly diffusion controlled process. This work provides significant in-sight in to the important area of storage, transport, and in delivering ionic drug payload with time using Mg–Al LDH materials.

Acknowledgements

The authors are grateful to the Director, Central Glass and Ceramic Research Institute, Kolkata, India for providing the permission to carry on the above work. Thanks are due to all other support staffs of CGCRI, Kolkata who made this work possible. Authors thank IIT, Kharagpur for low angle X-ray diffraction studies. We are indeed indebted to the CSIR Network Program NWP 0035 for all the kind support and the financial assistance for undertaking this work.

References

[1] P.P. Yang, Z.W. Quan, C.X. Li, X.J. Kang, H.Z. Lian, J. Lin, Bioactive, luminescent and mesoporous europium-doped hydroxyapatite as a drug carrier, Biomaterials 29 (2008) 4341–4347.
[2] R.S. Soumya, S. Ghosh, E.T. Abraham, Preparation and characterization of guar gum nanoparticles, Int. J. Biol. Macromol. 46 (2010) 267–269.
[3] C.M. Zhang, C.X. Li, C. Peng, R.T. Chai, S.S. Huang, D.M. Yang, Z.Y. Cheng, J. Lin, Facile and controllable synthesis of monodisperse CaF_2 and CaF_2:Ce^{3+}/Tb^{3+} hollow spheres as efficient luminescent materials and smart drug carriers, Chem. Eur. J. 16 (2010) 5672–5680.
[4] S. Ghosh, D. Carty, S.P. Clarke, S.A. Corr, R. Tekoriute, Y.K. Gun'ko, D.F. Brougham, NMR studies into colloidal stability and magnetic order in fatty acid stabilised aqueous magnetic fluids, Phys. Chem. Chem. Phys. 12 (2010) 14009–14016.
[5] J.K. Stolarczyk, S. Ghosh, D.F. Brougham, Controlled growth of nanoparticle clusters through competitive stabilizer desorption, Angew. Chem. Int. Ed. 48 (2009) 175–178.
[6] S.L. Gai, P.P. Yang, C.X. Li, W.X. Wang, Y.L. Dai, N. Niu, J. Lin, Synthesis of magnetic, up-conversion luminescent, and mesoporous core–shell-structured nanocomposites as drug carriers, Adv. Funct. Mater. 20 (2010) 1166–1172.
[7] S.S. Huang, Y. Fan, Z.Y. Cheng, D.Y. Kong, P.P. Yang, Z.W. Quan, C.M. Zhang, J. Lin, Magnetic mesoporous silica spheres for drug targeting and controlled release, J. Phys. Chem. C 113 (2009) 1775–1784.
[8] P.P. Yang, Z.W. Quan, Z.Y. Hou, C.X. Li, X.J. Kang, Z.Y. Cheng, J. Lin, A magnetic, luminescent and mesoporous core–shell structured composite material as drug carrier, Biomaterials 30 (2009) 4786–4795.
[9] A.I. Khan, L.X. Lei, A.J. Norquist, D. O'Hare, Intercalation and controlled release of pharmaceutically active compounds from a layered double hydroxide, Chem. Commun. 234 (2001) 2–2343.
[10] V. Rives, Characterisation of layered double hydroxides and their decomposition products, Mater. Chem. Phys. 75 (2002) 19–25.
[11] S.V. Prasanna, P.V. Kamath, C. Shivakumara, Synthesis and characterization of layered double hydroxides (LDHs) with intercalated chromate ions, Mater. Res. Bull. 42 (2007) 1028–1039.
[12] C. Gerardin, D. Kostadinova, B. Coq, D. Tichit, LDH nanocomposites with different guest entities as precursors of supported Ni catalysts, Chem. Mater. 20 (2008) 2086–2094.
[13] A.I. Khan, A. Ragavan, B. Fong, C. Markland, M. O'Brien, T.G. Dunbar, G.R. Williams, D. O'Hare, Recent developments in the use of layered double hydroxides as host materials for the storage and triggered release of functional anions, Ind. Eng. Chem. Res. 48 (2009) 10196–10205.
[14] T. Kameyama, K. Okazaki, K. Takagi, T. Torimoto, Stacked-structure-dependent photoelectrochemical properties of CdS nanoparticle/layered double hydroxide (LDH) nanosheet multilayer films prepared by layer-by-layer accumulation, Phys. Chem. Chem. Phys. 11 (2009) 5369–5376.
[15] J.H. Lee, S.W. Rhee, H.J. Nam, D.Y. Jung, Surface selective deposition of PMMA on layered double hydroxide nanocrystals immobilized on solid substrates, Adv. Mater. 21 (2009) 546–549.
[16] A.L. Maciuca, E. Dumitriu, F. Fajula, V. Hulea, Mild oxidation of tetrahydrothiophene to sulfolane over V-, Mo- and W-containing layered double hydroxides, Appl. Catal. A 338 (2008) 1–8.
[17] B.F. Sels, D.E. De Vos, P.A. Jacobs, Kinetics of the oxygenation of unsaturated organics with singlet oxygen generated from H_2O_2 by a heterogeneous molybdenum catalyst, J. Am. Chem. Soc. 129 (2007) 6916–6926.
[18] S. Sun, W.G. Hou, The photoluminescence of Co–Al-layered double hydroxide, Chin. Chem. Lett. 18 (2007) 1371–1373.
[19] D.P. Yan, J. Lu, M. Wei, D.G. Evans, X. Duan, Sulforhodamine B intercalated layered double hydroxide thin film with polarized photoluminescence, J. Phys. Chem. B 113 (2009) 1381–1388.
[20] J.M. Oh, M. Park, S.T. Kim, J.Y. Jung, Y.G. Kang, J.H. Choy, Efficient delivery of anticancer drug MTX through MTX–LDH nanohybrid system, J. Phys. Chem. Solids 67 (2006) 1024–1027.
[21] J. Jung, I.H. Lee, E. Lee, J. Park, S. Jon, pH-sensitive polymer nanospheres for use as a potential drug delivery vehicle, Biomacromolecules 8 (2007) 3401–3407.
[22] J.I. Bilbao, E. de Luis, J.A.G. de Jalon, A. de Martino, M.D. Lozano, A.M. de la Cuesta, B. Sangro, Comparative study of four different spherical embolic particles in an animal model: a morphologic and histologic evaluation, J. Vasc. Interv. Radiol. 19 (2008) 1625–1638.
[23] B.D. Chithrani, A.A. Ghazani, W.C.W. Chan, Determining the size and shape dependence of gold nanoparticle uptake into mammalian cells, Nano Lett. 6 (2006) 662–668.
[24] S. Muro, C. Garnacho, J.A. Champion, J. Leferovich, C. Gajewski, E.H. Schuchman, S. Mitragotri, V.R. Muzykantov, Control of endothelial targeting and intracellular delivery of therapeutic enzymes by modulating

the size and shape of ICAM-1-targeted carriers, Mol. Ther. 16 (2008) 1450–1458.
[25] E. Wisse, F. Braet, D.Z. Luo, R. DeZanger, D. Jans, E. Crabbe, A. Vermoesen, Structure and function of sinusoidal lining cells in the liver, Toxicol. Pathol. 24 (1996) 100–111.
[26] F. Yuan, M. Dellian, D. Fukumura, M. Leunig, D.A. Berk, V.P. Torchilin, R.K. Jain, Vascular-permeability in a human tumor xenograft—molecular-size dependence and cutoff size, Cancer Res. 55 (1995) 3752–3756.
[27] Y. Kuang, L. Zhao, S. Zhang, F. Zhang, M.D. Dong, S.L. Xu, Morphologies, preparations and applications of layered double hydroxide micro-/nanostructures, Materials 3 (2010) 5220–5235.
[28] Z.P. Xu, G. Stevenson, C.Q. Lu, G.Q. Lu, Dispersion and size control of layered double hydroxide nanoparticles in aqueous solutions, J. Phys. Chem. B 110 (2006) 16923–16929.
[29] M. Chakraborty, S. Dasgupta, C. Soundrapandian, J. Chakraborty, S. Ghosh, M.K. Mitra, D. Basu, Methotrexate intercalated ZnAl-layered double hydroxide hybrid, J. Solid State Chem. 184 (2011) 2439–2445.
[30] S.C. Tjong, H. Chen, Nanocrystalline materials and coatings, Mater. Sci. Eng. Rep. 45 (2004) 1–88.
[31] S. Ghosh, D. Divya, K.C. Remani, T.S. Sreeremya, Growth of monodisperse nanocrystals of cerium oxide during synthesis and annealing, J. Nanopart. Res. 12 (2010) 1905–1911.
[32] B.X. Li, J. He, D.G. Evans, X. Duan, Inorganic layered double hydroxides as a drug delivery system—intercalation and in vitro release of fenbufen, Appl. Clay Sci. 27 (2004) 199–207.
[33] M. Chakraborty, S. Dasgupta, P. Bose, A. Misra, T.K. Mandal, M. Mitra, J. Chakraborty, D. Basu, Layered double hydroxide: inorganic organic conjugate nanocarrier for methotrexate, J. Phys. Chem. Solids 72 (2011) 779–783.
[34] A.W. Musumeci, Z.P. Xu, S.V. Smith, R.F. Minchin, D.J. Martin, Layered double hydroxide nanoparticles incorporating terbium: applicability as a fluorescent probe and morphology modifier, J. Nanopart. Res. 12 (2010) 111–120.
[35] H.C. Greenwell, L.A. Bindley, P.R. Unwin, P.J. Holliman, W. Jones, P.V. Coveney, S.L. Barnes, In situ monitoring of crystal growth and dissolution of oriented layered double-hydroxide crystals immobilized on silicon, J. Cryst. Growth 294 (2006) 53–59.
[36] O.C. Wilson, T. Olorunyolemi, A. Jaworski, L. Borum, D. Young, A. Siriwat, E. Dickens, C. Oriakhi, M. Lerner, Surface and interfacial properties of polymer-intercalated layered double hydroxide nanocomposites, Appl. Clay Sci. 15 (1999) 265–279.
[37] A.V. Radha, G.S. Thomas, P.V. Kamath, C. Shivakumara, Suppression of spinel formation to induce reversible thermal behavior in the layered double hydroxides (LDHs) of Co with Al, Fe, Ga, and In, J. Phys. Chem. B 111 (2007) 3384–3390.
[38] S.I. Stupp, P.V. Braun, Molecular manipulation of microstructures: biomaterials, ceramics, and semiconductors, Science 277 (1997) 1242–1248.
[39] G.M. Lombardo, G.C. Pappalardo, Thermal effects on mixed metal (Zn/Al) layered double hydroxides: direct modeling of the X-ray powder diffraction line shape through molecular dynamics simulations, Chem. Mater. 20 (2008) 5585–5592.
[40] X.F. Zhao, F.Z. Zhang, S.L. Xu, D.G. Evans, X. Duan, From layered double hydroxides to ZnO-based mixed metal oxides by thermal decomposition: transformation mechanism and UV-blocking properties of the product, Chem. Mater. 22 (2010) 3933–3942.
[41] N. Yamaguchi, D. Ando, K. Tadanaga, M. Tatsumisago, Direct formation of Mg–Al-layered double-hydroxide films on glass substrate by the sol–gel method with hot water treatment, J. Am. Ceram. Soc. 90 (2007) 1940–1942.
[42] L.C. Costello, R.B. Franklin, P. Feng, Mitochondrial function, zinc, and intermediary metabolism relationships in normal prostate and prostate cancer, Mitochondrion 5 (2005) 143–153.
[43] J.H. Choy, J.S. Jung, J.M. Oh, M. Park, J. Jeong, Y.K. Kang, O.J. Han, Layered double hydroxide as an efficient drug reservoir for folate derivatives, Biomaterials 25 (2004) 3059–3064.
[44] B.S. Dave, A.F. Amin, M.M. Patel, Gastroretentive drug delivery system of ranitidine hydrochloride: formulation and in vitro evaluation, AAPS Pharm. Sci. Tech. 5 (2004) e34.